Istraživanja i projektovanja za privredu
ISSN 1451-4117
DOI:10.5937/jaes0-48184
www.engineeringscience.rs

iipp publishing

Journal of Applied Engineering Science
Vol. 22, No. 1, 2024
Original Scientific Paper
Paper number: 22(2024)1, 1177, 171-183

DEVELOPMENT OF A FEM PROCEDURE FOR EVALUATING THE PRESSURE PROFILE IN THE INDUSTRIAL WHEEL AND FATIGUE STRENGTH ANALYSES

Nicola Danzi, Luigi Solazzi*, Michele Cima

Brescia University (Università degli Studi di Brescia), Department of Industrial and Mechanical Engineering, Via Branze 38, Italy

** luigi.solazzi@unibs.it*

Industrial wheels are heavily loaded components that undergo severe cyclic stress conditions. Thus, the design of the rims must include a wide fatigue study which articulates in laboratory and field tests, analytical and numerical analyses and comparison of the experimental and computational results. This paper presents the study approach applied in the study of a 25 in rim for earth-moving machines manufactured by Moveero. The rim was subject to a design update which provided the reduction of the thickness from 11 mm to 9 mm. We decided to study the interaction tire-rim because it's a critical zone. The failures affected the area of the seat radius of the fixed flange of the rim, which resulted to be the most stressed part of the rim because of the bending actions of the tire on the flange. In order to deepen the cyclic mechanical behaviour of the component, laboratory inflation and rolling tests were carried out in Woodridge USA considering several combinations of inflation pressure and radial load applied to the wheel. The strain data from the tests were analysed to develop a reverse empirical model for the contact pressure between tire and rim. Once the load diagram applied to the flange for each test was estimated, FEM static simulations could be performed on a 3D model of the rim through SolidWorks Simulation. The stress fields obtained were then used for fatigue FEM numerical analyses which could return an evaluation of the predicted life of the component under several load conditions.

Keywords: fatigue, industrial wheel, FEM analysis, wheel stress profile, material fatigue parameter

1 INTRODUCTION

The goal of this article is the fatigue study of a wheel rim for earthmoving vehicles [1], [2]. In particular, we want to identify the distribution of loads acting on the fixed flange (Fig. 1) due to rolling, starting from results obtained from laboratory tests. After having highlighted the best distribution of pressures, we proceed with numerous finite element analyses from which it was possible to evaluate the influence of different parameters, such as the vertical load, the inflation pressure and the type of tire.

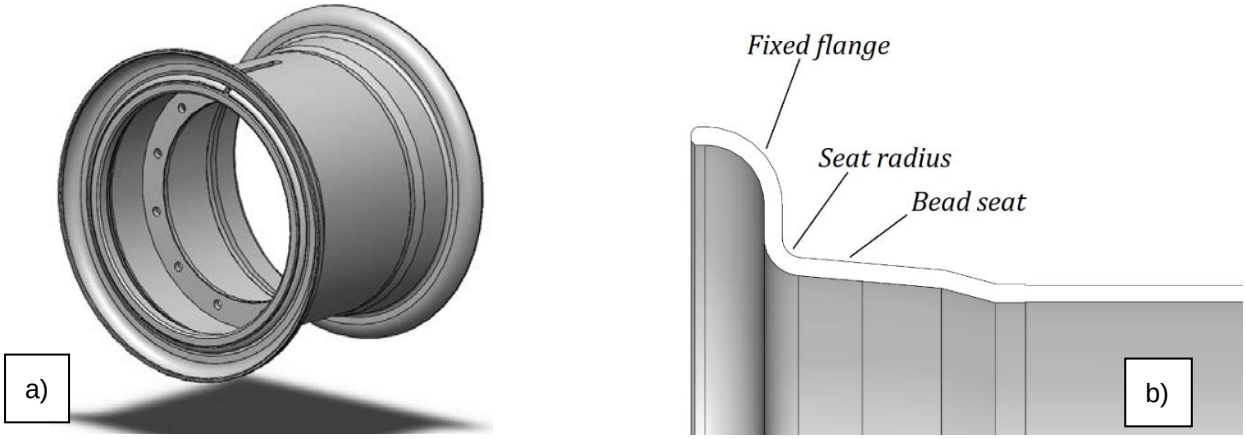

Fig. 1. a) Image of the component object of this study; b) Reference areas of the rim

The wheel under study is produced by Moveero and it is mainly used on wheel loaders. This is defined by the code 25-19.5/2.5 (in inches), where the first number indicates the rim diameter, the second is the depth of the rim channel (i.e., the maximum width available for housing the tire, measured on the median transverse plane) and the third is the height of the edge of the rim. This wheel is composed of four elements:

- the base of the rim: made of two components welded together with the submerged arc welding process along the circumferential direction;
- an elastic ring: with the task of keeping all the components of the wheel assembled;
- two lateral flanges: with the task of containing the tire beads (one fixed and one removable to facilitate the replacement of the tire).

The portion that undergoes the greatest stress due to interaction with the tire is the fixed flange, which can be divided into the zone shown in Fig. 1b:

- bead seat, which is a 5° inclined area where the tire bead rests;
- Seat radius, which is the radius of connection between the seat of the tire bead and the vertical wall of the edge of the flange;
- fixed flange, this area consists of a vertical wall and a subsequent radius of connection with the horizontal end of the flange.

The main loads to which the wheel is subjected can be due to tire inflation pressure and radial load, due to the weight supported by the wheel [3]. The pressure inside the tire supports the weight of the car and pushes the beads inside their seat against the flanges. This generates an additional load on the rim due to the pressurized air. The inflation pressure acts directly on the outer side of the rim and indirectly on the flange, by pushing on the beads. The air, which pushes on the sidewalls of the tire, generates a lateral load, which acts in the axial direction. This force varies depending on the type of tire, the proportion of its cross section, and its reinforcements [4]. Precisely the complexity of the load conditions on the fixed flange, in particular in the radius area, makes it difficult to estimate the fatigue life of this component.

2 TEST ON FIELD

Laboratory tests were carried out in the Woodridge laboratory (USA) where the wheel was subjected to rolling tests with radial load. The rim has undergone several tests with the use of both radial and bias tires. To detect the stresses on the flange, HBK model 1-LY1x-3/350A [5] strain gauges were applied and placed on the radius of the flange, which is the most stressed area [6]–[8]. In particular, the positioning was carried out starting from the centre of the beam (F2) and then the adjacent strain gauges were placed as a continuation based on the size of the grid (Fig. 2a), obtaining the configuration shown in Fig. 2b.

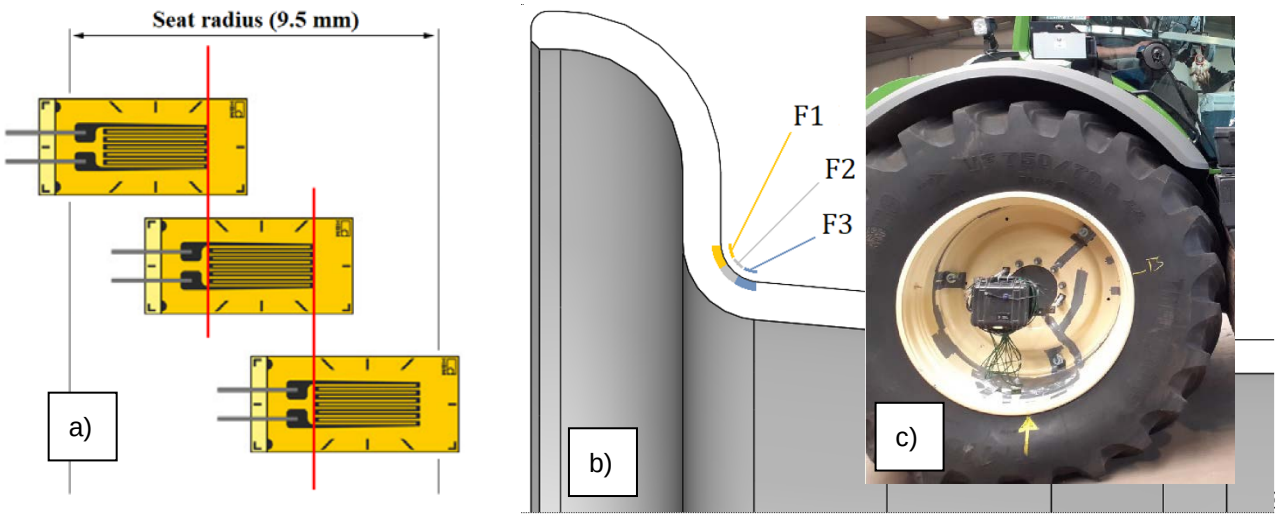

Fig. 2. a) Representation of the methodology for arranging the strain gauges on the radius of the flange being studied; b) Qualitative representation of the positions of the strain gauges along the flange; c) Application of the strain gauges on the radius of the flange

The points object of this analysis is F1, F2 and F3 strains because are the nearest to the critical zone (see Fig. 2b), where the strain gauges indicated with F refer to the fixed flange. The test sequence was the following for each type of tire:

- application of the strain gauges as shown in Fig. 2b on the seat radius surface both on the removable flange side and on the fixed flange one;
- strain gauges connection to the SOMAT E-DAQ Lite acquisition unit, acquired at 1'000 sample per second;
- inflation of the tire with detection of deformation measurements given by the strain gauges;
- application of stepped loads and detection of strain gauge data;
- deflation of the tire and verification of zero settings of the strain gauges;

This procedure was repeated for four pressure values, such as 2 bar, 4 bar, 6 bar and 8 bar, in order to detect a possible connection between the breakages that occurred during operation and the tire inflation pressure. The technicians started from the highest-pressure value and applied five different radial loads, respectively of 5.000 kg, 7.500 kg, 10.000 kg, 12.500 kg and 15.100 kg, up to the test with 2 bar where the test was concluded with a maximum applied load of 12.500 kg [9], [10].

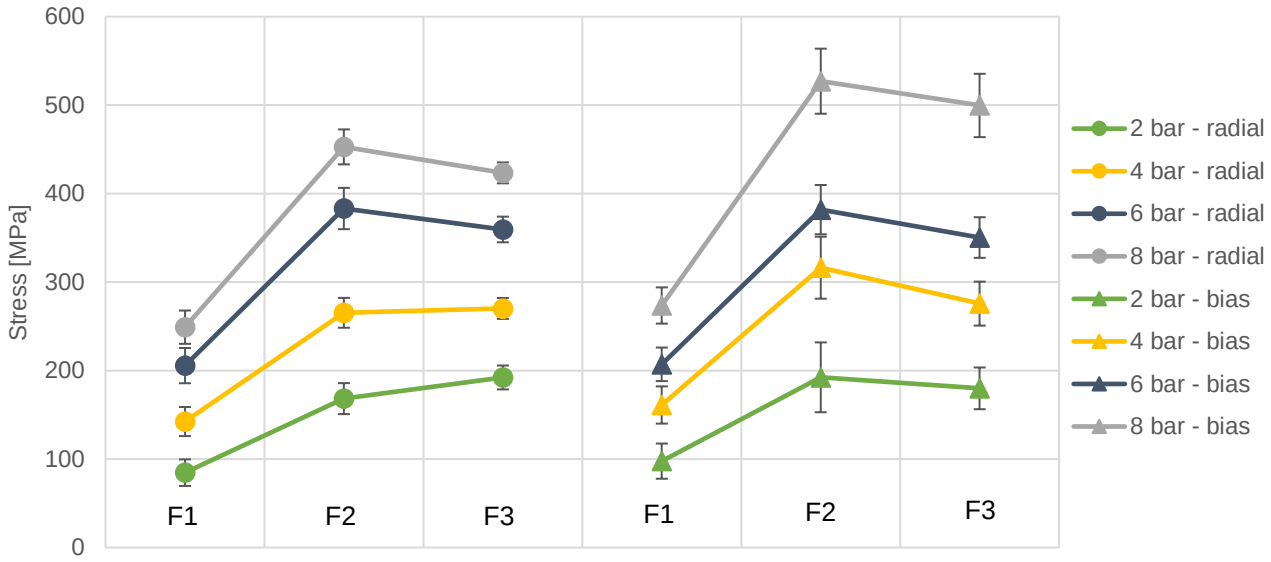

Fig. 3. Average results of stress values, referred to a specific pressure value, for different radial loads measured by the strain gauges on the fixed flange when using radial and bias tires

From Fig. 3, it can be seen that the stresses of strain gauges F2 and F3 are higher than F1, for each test. In addition, it is possible to identify how the bias tire transfers a greater load to the flange. It can be seen that radial tire stresses the F3 position more up to a pressure of 4 bar and then the F2 position up to 8 bar, while the bias stresses the F2 position more for each level of pressure, demonstrating a different load distribution due to the configuration of the tire mounted on the rim. For these reasons, this paper examined positions F2 and F3, which represent the most critical area of the fixed flange.

3 EXPERIMENTAL MODEL

The equations (1) and (2) are commonly used in the automotive industry to evaluate the load applied to the rim flange (Fig. 4a) as a function of the inflation pressure [11], [12]. They are based on a simple balance of the forces acting on the internal lateral surface of the tire and the ones applied to the external surface of the tire seat by the rim flange, so they are an approximation of the real structure. In equations (1) and (2), a is the tire radius [mm], r_f is the radius of the load point on the rim flange [mm], P_0 is the tire inflation pressure [MPa], W_p is the axial component of the force due to the inflation pressure [N] and T_f is the load per unit of circumferential length of the single rim flange [N/mm].

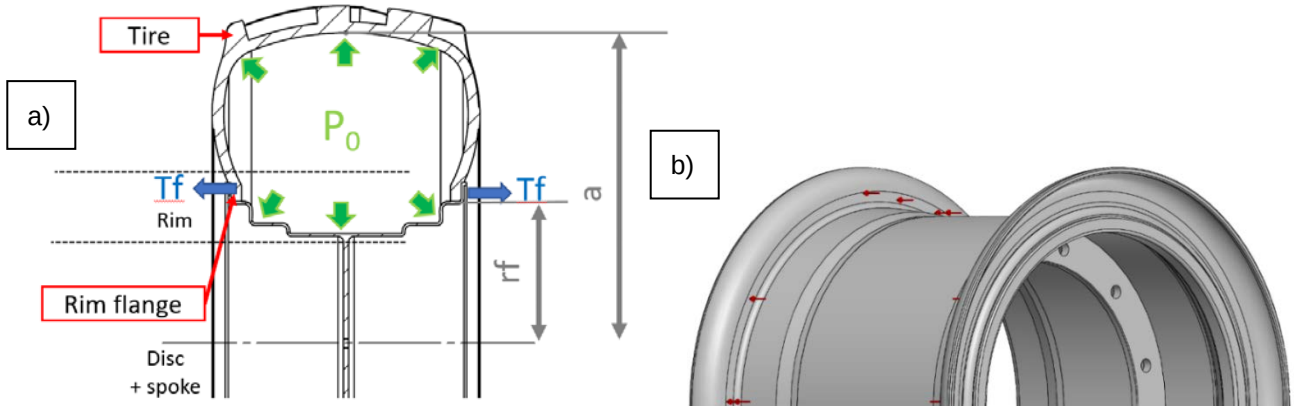

Fig. 4. a) Load condition on the rim due to tire inflation; b) Application of the predicted load applied to the flange surface

$$W_p = \pi\left(a^2 - r_f^2\right)P_0 \quad [N] \tag{1}$$

$$T_f = \frac{W_p}{2 \cdot 2 \cdot \pi \cdot r_f} = \left(a^2 - r_f^2\right)\frac{P_0}{4r_f} \quad [^{N}/_{mm}] \tag{2}$$

The ratio of flange load to bead seat load is considered to vary depending on the contact conditions at the tire-rim interface [13]. This is influenced by the type of tire (geometry and material), the inflation pressure, and the design of the rim [14], [15]. This model was firstly applied to the study of the inflation problem [16] to estimate if it could predict the experimental measurements from laboratory [17]. The axial load provided by the automotive theory was applied to the flange surface of the rim 3D model, as shown in Fig. 4b.

A Finite Element Method (FEM) simulation could then be performed on the model; the results expected from the analysis in order to confirm the suitability of the automotive theory formulas should have been in good accordance with the laboratory measurements. However, a good match between the experimental results and the stress field predicted by the automotive theory could not be found. The study based on the automotive theory formulas was therefore abandoned [18], [19]. A second option for developing a direct model of the tire-rim interaction was to simulate it through a FEM model of the entire wheel, where information about the contact pressure distribution on the tire-rim interface [20]–[22] was sought. However, this approach was affected by many limitations, since accurate information on the design of the tire were not available [23], [24]. Even nowadays, tire structure modelling and analysis represent a challenging operation as non-linearity occurs in the material properties as well as in the contact boundary conditions. Moreover, the tread pattern, the complex and composite internal tire design and their influence on the load distribution must be considered [25]. In the case of our study, the non-linear and anisotropic mechanical behaviour of a composite component could not be modelled, especially because of the lack of information on the disposition of the carcass wire and on the tread design. For these reasons, modelling the tire through finite elements was not considered as an option. Generally speaking, developing a direct model of the tire-rim contact phenomenon turned out to be challenging [25], [26]. In fact, the complexity of a direct modelling approach not only lies in creating the model, but especially in tuning it on the experimental results from the laboratory tests. In our case, matching the experimental data as accurately as possible was necessary to obtain the most reliable evaluations in the fatigue FEM analyses. For these reasons, any direct modelling of the phenomenon was excluded and a reverse approach was adopted instead. Therefore, experimental data from laboratory tests were not used as a comparison term to validate a direct model, but were considered as a starting point of analysis.

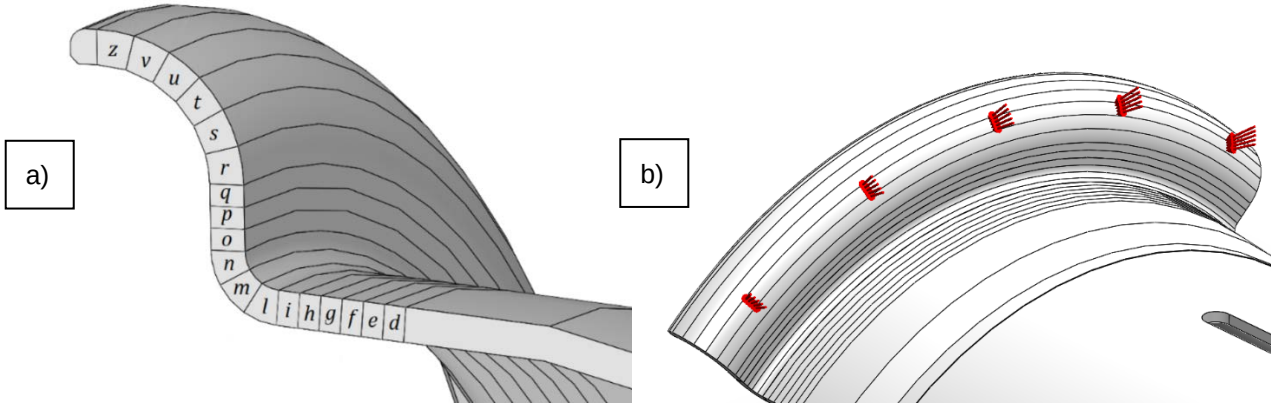

Fig. 5. a) Discretization adopted for the fixed flange surface; b) example of load condition applied in the FEM

More in detail, attempts of solutions for the contact pressure distribution were supposed and numerically simulated until a good match between the FEM solutions and the experimental evidence could be found. To simplify the pressure distribution assumption process, the surface area of the 3D rim model was discretized into the flange area (Fig. 5a). Dividing the surface into portions over each of which a uniform normal pressure can be applied has greatly simplified the formulation of contact pressure solutions. The first step of this process was to study the influence of each loaded area on the shape of the stress curve in the seat radius. To do this, each portion of the flange was individually loaded as shown in Fig. 5b and the stress solution derived from the FEM simulation was recorded (Fig. 6). The main significance of this study did not lie in the magnitude of the detected stresses, but in the shape of the stress curve, i.e., the ratios of stresses recorded on the surfaces corresponding to the instrumented areas F1, F2 and F3. Thus, reproducing within FEM simulations the experimental results would have meant finding a linear combination of loaded flange areas. Knowing how each area (when loaded) affects the shape of the stress curve greatly simplifies the attempt process. It is important that the application of a linear combination of pressure was possible only thanks to the hypothesis of linear elastic mechanical field in which the material was supposed to be. Only under this condition, in fact, the principle of superposition could be applied. Although studying the effect of each individual flange area was extremely useful to understand how to tune the model, it could not be considered sufficient to systematically assume a large number of solutions for contact pressure.

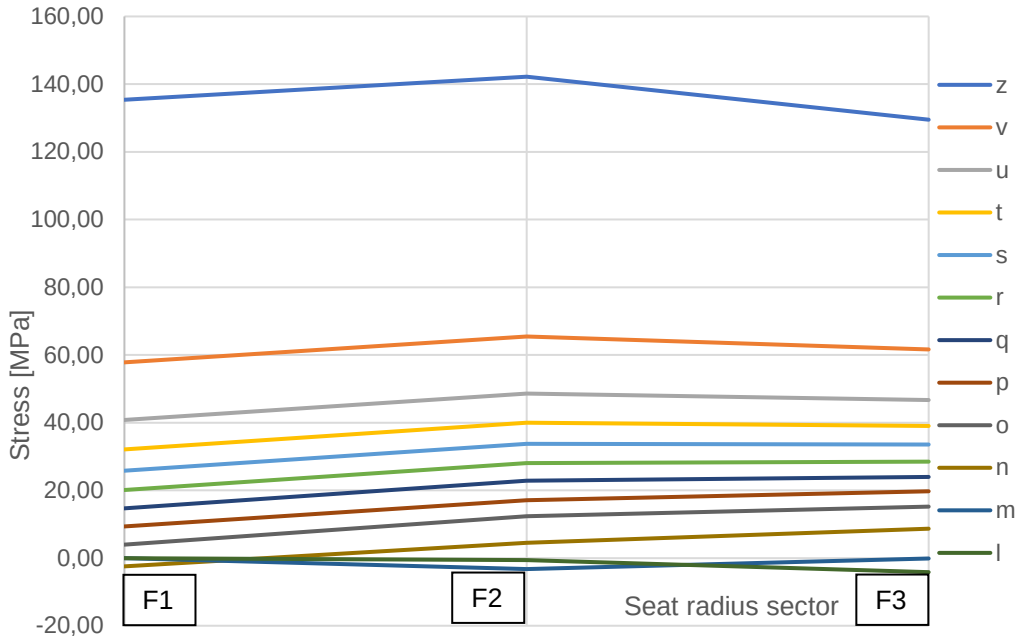

Fig. 6. FEM-recorded stress curve in the seat radius for each loaded flange area

So, experimental data from the theory provided by the tire manufacturer were then adapted to the discretization of the Moveero rim model. As an example, the measured pressure distribution for the 3,2-bar inflation case and fitted to the discretized model is presented in Fig. 7. The further step of the study would be to adjust the pressure diagram for each inflation and radial load configuration tested, trying to fit our profile with this one performed by the manufacturer, trying only to shift on the X axis our pressure profile. This is done to have a convergence between experimental data and numerical simulation, checking the stresses in the point where we have placed strain gauge.

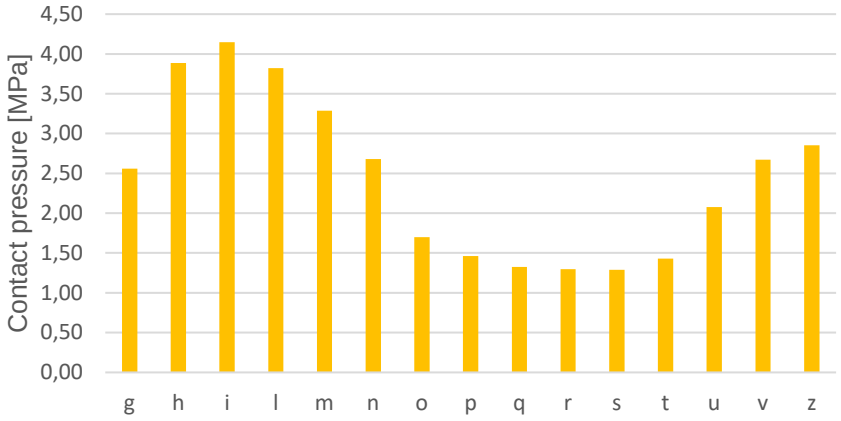

Fig. 7. Contact pressure distribution (3,2-bar inflation)

4 MODULATION OF THE SIGNALE AND MODEL VALIDATION TUNING

As stated before, a tuning of the pressure distribution obtained by the manufacturer study was needed in order to reproduce the stress state measured during the laboratory tests for each load configuration (Fig. 8). The adjustment of the load diagram consisted in modulating the amplitude of the peak of each different portion of the fixed flange, starting from the profile performed by the manufacturer Fig. 7, for every inflation pressure considered.

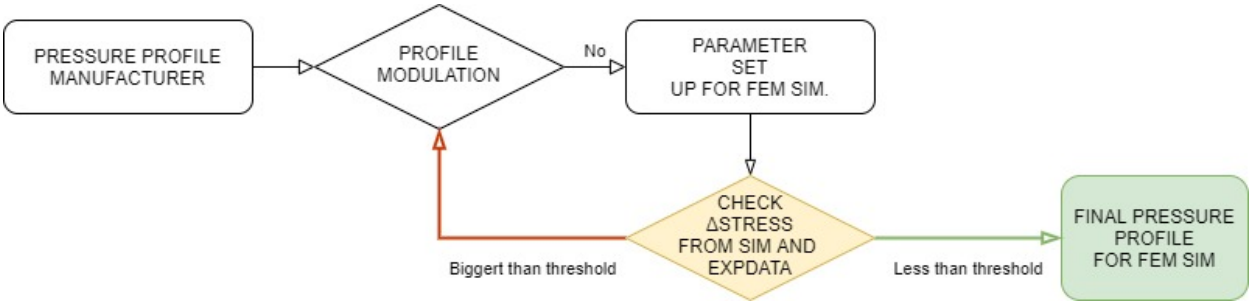

Fig. 8. Flow chart of tunning process

The tuning of the reverse model was done by varying and comparing the contact pressure diagram provided by finite element analyses and the one given by the experimental evidence. The model and the mesh used for these simulations are shown in Fig. 9a and Table 1. The mesh was obtained after an accurate process of convergence in order to prevent even little inaccuracies in the predicted stress fields. Moreover, the model was simplified, as it was considered just one sector of the rim thanks to the axial-symmetry of both the component and of the load [27]. To do this, sliding boundaries were applied to the model (Fig. 9b). Finally, the stress field acquired by the simulations could vary depending on the load conditions, but generally reported a highly stressed area coinciding with the seat radius (Fig. 10a). In fact, the more intense the pressure applied to the flange area, the darker the colour associated.

Table 1. Mesh parameters applied to the 3D rim model to perform the fatigue FEM analysis

Nodes number	1.453.924
Elements number	1.009.933
Element type	Solid CST
Minimum element size – seat radius area	1 mm
Maximum element size	40 mm

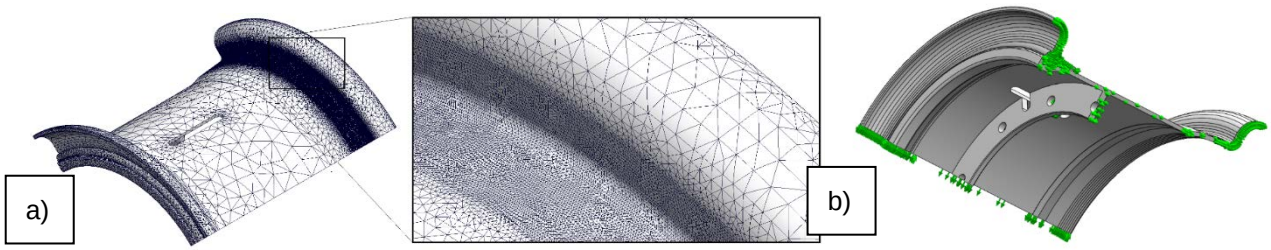

Fig. 9. a) 3D model and mesh used for the simulations; b) Axial symmetry constraints

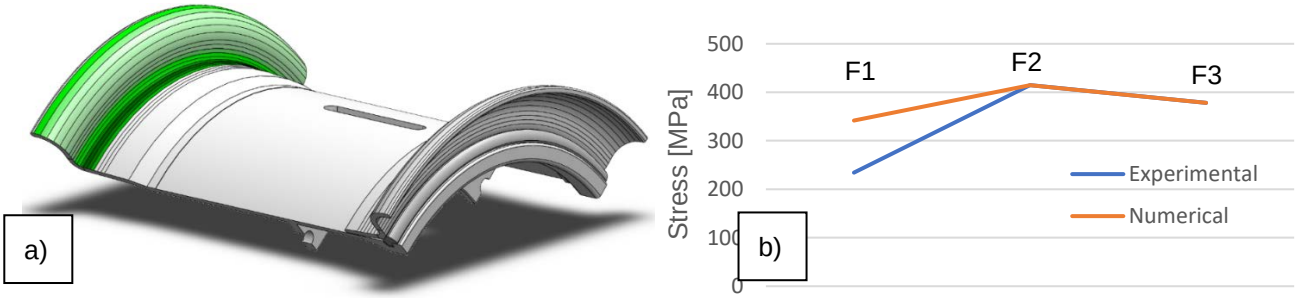

Fig. 10. a) Qualitative representation of the mean pressure diagram applied in the simulations; b) Comparison between experimental and numerical results (Fig. 11c) for the radial tire – 6 bar – 12.500 kg configuration

As shown in Fig. 10b, a good match between the experimental and numerical results of the F2 and F3 areas could be found. On the other hand, F1 is the only one for that we can't find a correspondence on the model. This was likely due both to inaccuracies in the manual positioning and manual alignment of the strain gauges, which could cause the strain gauges to record transversal strain [28] and to excessive model approximation. In any case, being the F1 stress the lower of the three recorded, this did not represent a big limitation.

The iterative process of solution hypothesis was performed for each load configuration until errors above a few percentile points were obtained, leading to the possible solutions for the contact problem (Fig. 11).

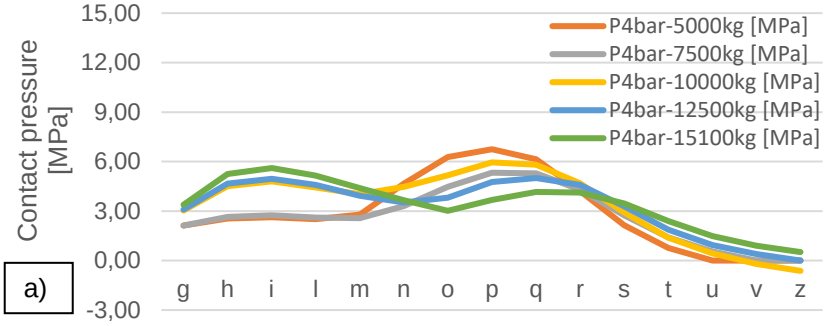

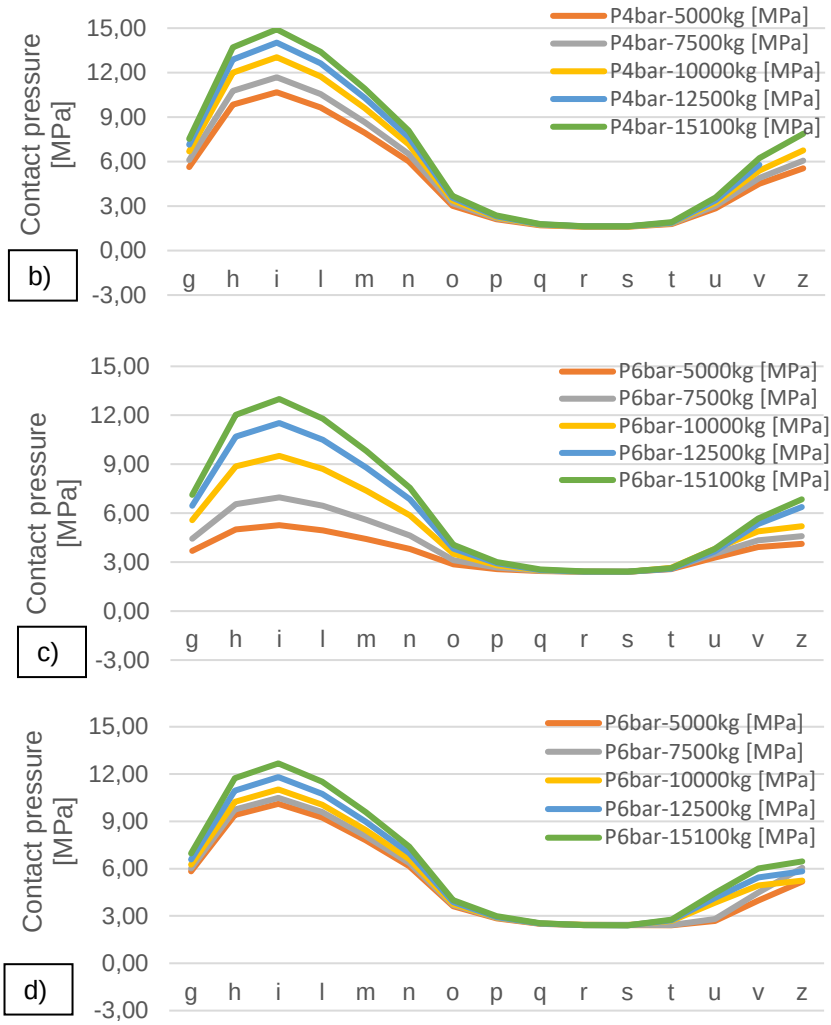

Fig. 11. Possible solutions found for the tire-rim contact phenomenon. Load diagrams comparison: a) 4 bar – radial tire; b) 4 bar – bias tire; c) 6 bar – radial tire; d) 6 bar – bias tire

5 FATIGUE TESTS RESULTS

The stress fields calculated through the static FEM simulations described above were necessary both for a better comprehension of the tire-rim contact phenomenon and for the requirements of the software [29], [30]. In fact, SolidWorks Simulations needs a stress field from a static analysis in order to perform a fatigue one, as well as many other FEM software [31]. The fatigue analysis function of Solidworks® causes static stress results to vary between two extremes that, due to the nature of our study approach, are identified through the experimental analysis of load cycles. More in detail, the maximum and minimum stresses have been identified analytically from the load cycles recorded, which shape can be exemplified by the cycles reported in Fig. 12. Furthermore, the regularity of the cycle allowed to sample the maximum and minimum values manually for each load configuration.

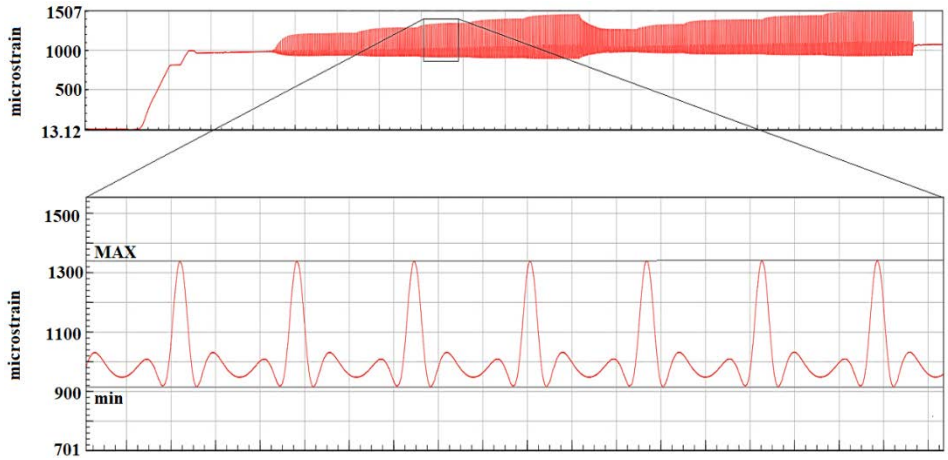

Fig. 12. Example of the process of sampling of the cycles from the strain gauges recording (4 bar – 7.500 kg – radial tire)

As described previously, the maximum stress value was needed as a reference to be reproduce in the static FEM simulations, while the minimum stress was used to calculate the experimental cycle ratio R (see eq. 3), which is required by the software in order to execute any fatigue analysis and must be defined by the user.

$$R = \frac{\sigma_{min}}{\sigma_{max}} \tag{3}$$

Once the stress fields were obtained in the static simulations for each of the load configurations, the fatigue FEM analysis could be performed (Fig. 13a). In order to perform any fatigue analyses the main instrument necessary was the *Wöhler* curve, obtained by a wide experimental campaign of fatigue experimental tests [32]. In our specific case of study, the *Wöhler* curve had to be identified in the curve associated with the most similar material from a dedicated database: for this study, the *Total Materia.* Since the mechanical problem related to the rim flange is purely flexural, the curves related to the bending alternated stress tests were considered. Structural steels were searched for among the *Total Materia* materials, as the steel used for the Moveero rim belongs to this category of materials. Considering the data provided by Moveero for the ultimate tensile strength, which is equal to about 370 MPa, the closest material found in the database was S235JR structural steel, which was taken as the reference. The flexural alternated fatigue curves found in *Total Materia* for this material is reported in Table 2 [33], [34].

Table 2. Wöhler experimental curve, provided by Total Materia, obtained under alternated symmetrical flexural load for structural steel S235JR

N	1.000	10.000	100.000	1.000.000
Stress [MPa]	324	266	219	180

Assuming this approach, a fatigue analysis was performed on the 3D model assuming S235JR steel as the material, while the model used for fatigue analysis of the component was the same as that used for static analyses. The fatigue life obtained from the FEM simulation was then compared with the experimental one to determine whether S235JR best approximates the real one [35], [36]. The numerical fatigue life evaluation was performed with reference to the 6 bar – 15.100 kg – radial tire configuration, as it is extremely similar to that applied to the failure test performed by the manufacturer (rolling speed 12.9 km/h) (Fig. 13b).

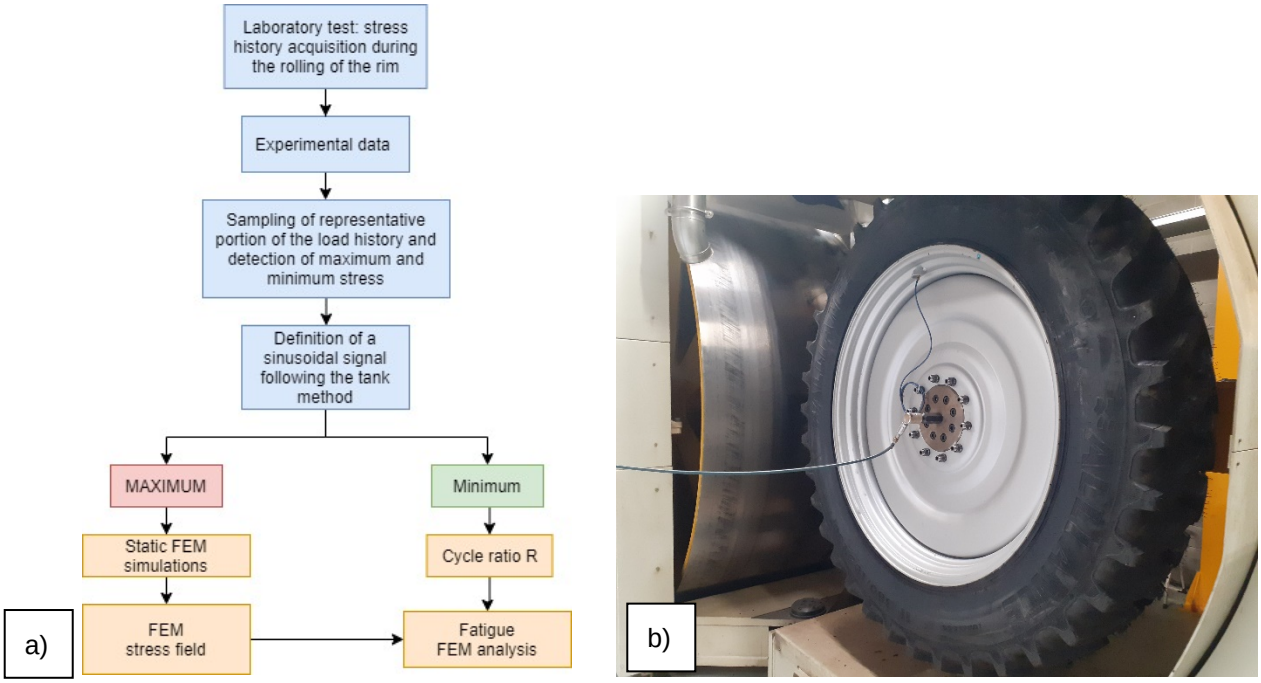

Fig. 13. a) Diagram of the workflow applied to the study; b) Example of a wheel during a rolling test

It must be remarked that, since one single rolling test was executed, this comparison must be considered purely indicative, as no statistical considerations can be done. However, based on the results shown in Table 3, it can be stated with good confidence that the S235JR represents the best approximation of the rim steel. Therefore, this material and the associated *Wöhler* curve were applied in the following fatigue analyses.

Table 3. Comparison of fatigue life assessment between rolling test and numerical test, where the cycles refer to a limited area of the component, i.e., the seat radius

N_f experimental	2.000.194
N_f numerical	2.332.000

Additional information needed to carry out fatigue simulations are the fatigue limit σ_{FA} and the method applied to correct the mean stress components σ_m of the cycle. As far as the fatigue limit is concerned, Total Materia reported a σ_{FA} equal to 180 MPa for the S235JR. In addition, σ_{FA} must be corrected with some coefficients (4) that take into account the forming process applied to the rim.

$$\sigma'_{FA} = k \cdot \sigma_{FA} \quad \text{with} \quad k = a \cdot {\sigma_R}^b \tag{5}$$

Where a and b are coefficients depending on the forming process applied to the material. As the steel sheet used for the rim production is hot rolled, corrective coefficients with the following values have been chosen:

$$a = 57{,}7 \quad b = -0{,}718 \tag{6}$$

By substituting the values given in (5) into (4), the following value for σ'_{FA} in (7) was found:

$$\sigma'_{FA} = 57{,}7 \cdot (370\ MPa)^{-0.718} \cdot 180 = 148{,}8\ MPa \tag{8}$$

This can be considered the corrected fatigue limit for the S235JR, which takes in account the process applied to the steel and, therefore, it was used in the following study analyses.

The last assessments needed before performing the fatigue FEM analyses regards the load cycle applied to the rim during its rotation. In fact, the loading cycle to which the rim is subject is not as simple as it could be thought, since the stress curve through the time is not a mere sinusoidal function. The strain gauges measurements analysed through the time axis, in fact, reveal a more complex trend, which is shown in Fig. 12. Here, two full strain cycles are clearly recognisable. A higher strain peak, which corresponds to the tire-ground contact, can be detected and it divides one cycle from the other. Lower peaks can be found between the higher peaks and they are generated by the particular tire-rim contact conditions that occur during the wheel rotation. Between the minor peaks, there is a relative minimum, which shows up when the rim point is in the higher position of the rotation, diametrically opposite to the tire-ground contact point.

What we had to investigate was the influence on the fatigue life of the minor peaks that occurs during the upper part of the rim rotation, opposite to the tire-ground contact point, in order to determine if the minor peaks affect the cumulative damage of the component. If the alternated stress point is located under the Haigh diagram line, its life influence can be considered negligible with a certain safety factor; if not, the component life should be considered affected, as the $\sigma_{a_{limF}}$ is exceeded. Before this check could be done, the stress values corresponding to the minor peaks must be collected.

This operation was done on the *nCode* graphs manually on samples of the cyclic load graph for each load condition. More in detail, the stress values associated to the maximum and the minimum of each cycle peak have been collected. The criterion used to detect the minimum points was based on the tank counting method [37]. From the "tank method" we have three different peaks for each cycle. Of course, the highest of the three peaks was already known to be influent on the life of the rim (highest alternated and average stress) so, the focus was set on the second and the third peak (orange and grey points in Fig. 14). As can be seen from the Haigh diagram in Fig. 14, the two cycles can be considered negligible in terms of cumulative damage. As an initial evaluation, the most burdensome loading conditions were inspected. In fact, if the highest cyclical stresses had been found to be irrelevant, the lowest would have been too. Thus, the most critical load condition for both the radial and the bias tire were examined, that is 6 bar – 15.100 kg case.

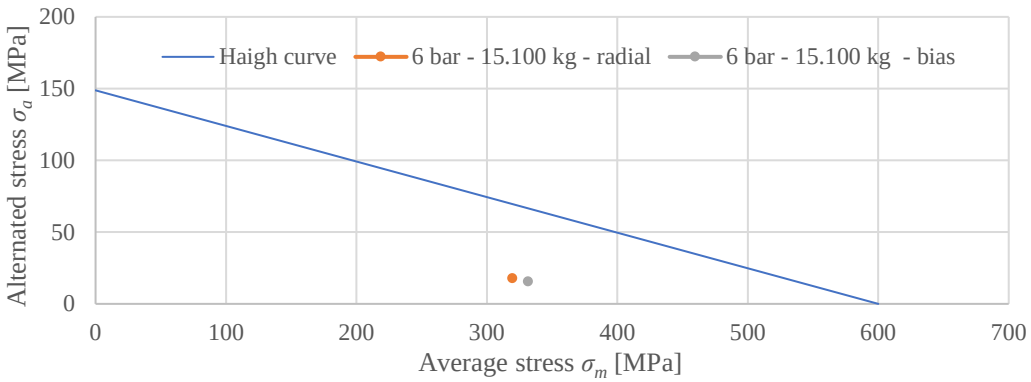

Fig. 14. S235 Haigh diagram of the points of the secondary peaks of the load cycle for the 6 bar – 15.100 kg configurations

Once the load cycle is found, all the fatigue study parameters have been evaluated and, thus, the FEM fatigue simulations can be executed. The software returns both predicted life and cumulative damage outputs, according to the Palmgren-Miner theory [38] – [42]. The analyses were performed for all load and tire design configurations available for inflation pressures of 4 and 6 bar. The 3D model and mesh used for this set of simulations are the same

presented in Table 1. The results obtained by the numerical analyses for the fatigue in terms of number of cycles are shown in Table 4.

Table 4. Predicted fatigue lives for each load and inflation condition from FEM numerical simulations

INFLATION P [bar]	TIRE DESIGN	RADIAL LOAD [kg]	CRITICAL AREA	R	σ_{max} [MPa]	N_f
4	Radial	5000	F3	0,851	279,0	Infinite
		7500	F3	0,830	290,8	Infinite
		10000	F3	0,796	299,6	Infinite
		12500	F2	0,653	308,7	Infinite
		15100	F2	0,618	318,3	Infinite
	Bias	5000	F2	0,776	318,7	Infinite
		7500	F2	0,730	335,3	Infinite
		10000	F2	0,682	353,4	301.900.000
		12500	F2	0,641	369,3	29.290.000
		15100	F2	0,602	387,2	3.168.000
6	Radial	5000	F2	0,836	388,0	Infinite
		7500	F2	0,804	400,1	Infinite
		10000	F2	0,764	415,7	142.600.000
		12500	F2	0,733	427,3	14.740.000
		15100	F2	0,708	439,3	2.174.000
	Bias	5000	F2	0,831	367,2	Infinite
		7500	F2	0,778	390,6	Infinite
		10000	F2	0,732	412,3	38.270.000
		12500	F2	0,695	434,1	2.763.000
		15100	F2	0,663	457,6	215.500

6 RESULT

The Fig. 11 shows the trend of the pressure we have on the rim when we change the inflation pressure, the radial load and the tire (radial or bias). The pressure profile is defined by iteration of numerical data obtained from FEM analysis triggered with experimental data acquired with strain gauges by test on field. This iteration is performed until we can reach a convergence in outcomes (Fig. 10b). The FEM are performed by sizing the rim in different slices (see Fig. 5a) and by applying to each a defined pressure and at the end checking the strain in the points where we have a certain data, in this way we can validate the FEM model.

This tuning procedure is necessary because what we can predict with different theories, in terms of profile pressure, is a first approximation of the pressure on the rim but every configuration is different (because of the combinations of some variables: geometry, tire, materials). The main deviation we may run into can be the maximum stress on the contact zone between rim and tire.

From the curves we obtained after the tuning process (Fig. 11) we can see as the radial load increases, the pressure increases in zone h, i and l unlike on zones near the flange (p, q, r, s, t) the contact pressure is marginally affected by the value of radial load. We can also observe that the tire type is a key factor on the curve. We find that by fixing the inflation pressure, for example 6 bar, the radial tire is more sensitive to the radial load than the bias one. This is clear from the Fig. 11 where it appears that the curves (mostly in the areas where the pressure is higher: h, i and l) are closer to each other so they are not so affected by a change in radial load applied. The curves (Fig. 11) are used for further numerical analysis to estimate the fatigue life of the component. Table 4 shows the result in the critical zones identified previously with the strain gauges 2 and 3 (F2 and F3 that in our model are on the radius zones that fall in the zone m, i and l). In detail the results show as the pressure of each type of tire and radial load varies the results in terms of maximum stress, cycle ratios and estimations of fatigue life.

In Fig. 15, the predicted lives are compared on a logarithmic scale with a maximum life of 10^7 cycles, which have been considered the infinite life limit. As it can be noticed, the only tire configuration which never shows limited predicted lives is the 4 bar – radial tire. For all the other tire configurations at least one case of predicted limited life occurs.

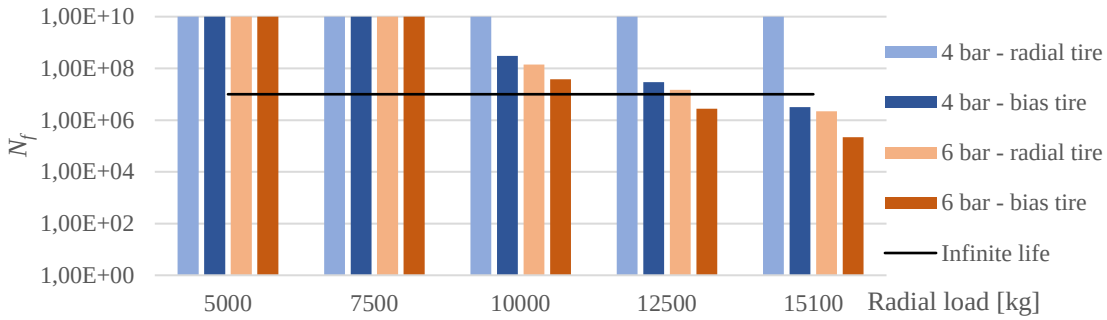

Fig. 15. Comparison of the component's predicted lives for all the tested load conditions

Another important parameter is the cycle stress ratio *R.* In fact, the higher the stress values, the highest the damage caused to the material. Moreover, the more the *R* ratio tends to zero, the more the cyclic stress can be approximated to a cycle pulsating from zero. This load condition can be considered far more critical compared to a cyclic stress with a *R* ratio which tends to 1, as it is closer to a static stress state. The influence of the combined maximum stress and cyclic ratio is shown in the Fig. 16 (the bigger the circle, the higher the predicted life), where the combination of these two parameters determines the cyclic damage of the rim.

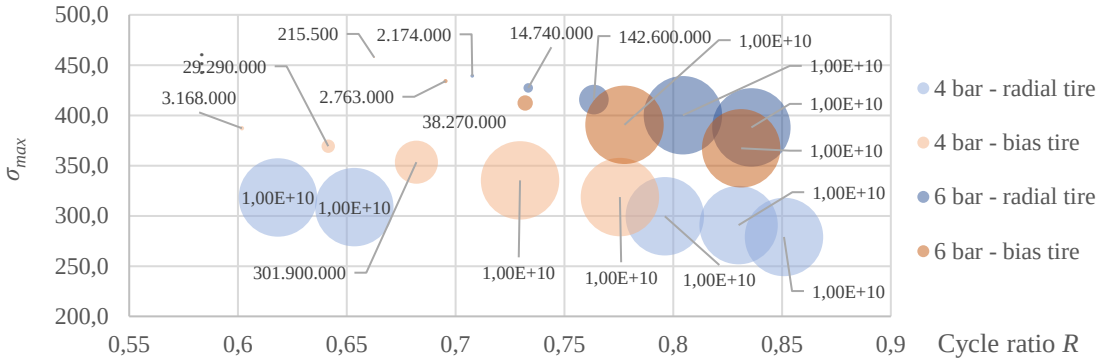

Fig. 16. Influence of combined maximum cycle stress ratio on expected life numerically

7 CONCLUSIONS

Direct modelling of the tire-rim contact pressure through mathematical or FEM tire models can hardly produce results which are accurately coherent with the experimental data, especially because the fatigue FEM analysis requires to process stress fields from static simulations as similar as possible to the experimental evidence in order to return good life predictions.

A reverse empirical model based on the iteration of attempts of solution for the contact pressure distribution between rim and tire in the rim flange area has been identified as the most suitable approach for the particular problem faced in this research. Following this modelling solution, the experimental results are not used as an empirical comparison term employed to verify the prediction of a direct model, instead they are considered as an experimental basis on which a reverse empirical model can be built. This particular model is not mainly intended to make predictions on the tire-rim interactions (even if many considerations on this phenomenon could be made thanks to it), but to reproduce the experimental results in the FEM numerical simulation in the most accurate way possible. Going backwards and analysing the solutions found for the pressure distributions, a deeper understanding of the phenomenon could be reached.

Previous measurement campaigns on the contact pressure distribution allowed us to realize that the most loaded areas are the bead seat and the flange hook ones. The static simulations revealed that the tire design affects the pressure distribution, as it was found that, especially for lower radial loads, bias tires tend to load more the upper areas of the flange hook compared to the radial ones, as confirmed by Moveero. The inflation pressure affects the load pattern as well, since the simulation results show that the less the tire is inflated, the less its deformed configuration is defined and, thus, the loaded area are not accurately identified as in the high-pressure configurations. Moreover, if the pressure distribution found in this study is considered reliable, it emerges that less inflated configurations can involve higher peaks in the contact pressure, as the deformed states of the tire are probably less rigid than the high inflated ones [43], [44].

The fatigue FEM simulations based on the static numerical results and on the hypotheses of neglecting the residual stresses of the material revealed that the critical load conditions are the high load configurations (12.500 kg and 15.100 kg). These load conditions are quite extreme and reasonably rarely reached by the structure during the exercise. Moreover, these radial loads have been simulated together with inflation pressures that exceed the value recommended by the tire manufacturers, that is 3,2 bar. Thus, these results must be considered as an evaluation of extremely hard load conditions and the limited life predictions must therefore be properly weighted. In any case, the

load conditions that eventually need further investigation and study are the ones mentioned above. Regarding the fatigue analyses, a wide experimental campaign for the cyclic characterization of the material is necessary in order to perform accurate fatigue predictions on the component. Another important step for the material characterization is studying the influence of the forming process on its mechanical properties, as both the residual stresses and the hardening can play an important role in the cyclical behaviour of the cold formed steel.

8 ACKNOWLEDGEMENT

The authors of this paper would like to thank engineers Bramè Giampietro and Mazzoni Alberto of Moveero company for the information provided for the development of this research.

9 REFERENCES

[1] A. Mazzoni and L. Solazzi, “Experimental field test on a multipiece steel wheel and influence of the material properties on its fatigue life evaluation,” Eng Fail Anal, vol. 135, p. 106106, May 2022, doi: 10.1016/j.engfailanal.2022.106106.

[2] J. M. E. Marques, L. Solazzi, and D. Benasciutti, “Fatigue Analysis of Nonstationary Random Loadings Measured in an Industrial Vehicle Wheel: Uncertainty of Fatigue Damage,” Metals (Basel), vol. 12, no. 4, p. 616, Apr. 2022, doi: 10.3390/met12040616.

[3] J.-P. Brüggemann et al., “Structural optimization of a wheel force transducer component for more realistic acquisition of vehicle load data and fracture mechanical evaluation,” Applications in Engineering Science, 2021, doi: 10.1016/j.apples.2020.100032.

[4] J. Stearns, T. Srivatsan, X. Gao, and P. C. Lam, “Understanding the influence of pressure and radial loads on stress and displacement response of a rotating body: The automobile wheel,” International Journal of Rotating Machinery, 2006, doi: 10.1155/IJRM/2006/60193.

[5] “HBK Strain gauges datasheet.” Accessed: Sep. 28, 2023. [Online]. Available: https://www.hbm.com/it/4561/ly-estensimetri-lineari-con-1-griglia-di-misura/?product_type_no=LY%20Estensimetri%20Lineari%20con%201%20Griglia%20di%20Misura

[6] S. B. P. Davoli, L. Vergani, S. Beretta, M. Guagliano, Costruzioni di macchine 1, 1st ed. McGraw-Hill Education, 2011.

[7] M. Cima and L. Solazzi, “Experimental and analytical study of random fatigue, in time and frequencies domain, on an industrial wheel,” Eng Fail Anal, 2020, doi: 10.1016/j.engfailanal.2020.105029.

[8] L. Solazzi and A. Mazzoni, “Experimental Study of the Fatigue Life of Off-Highway Steel Wheels Using the Rim Section Test Approach,” Applied Sciences, vol. 13, no. 16, p. 9119, Aug. 2023, doi: 10.3390/app13169119.

[9] “Biaxial Wheel Fatigue Test,” 2003.

[10] L. D. Nurkala and R. S. Wallace, “Development of the SAE biaxial wheel test load file,” in SAE Technical Papers, 2004. doi: 10.4271/2004-01-1578.

[11] T. Mizoguchi, H. Nishimura, K. Nakata, and J. Kawakami, “Stress analysis and fatigue strength evaluation of sheet fabricated 2-piece aluminum wheels for passenger cars.,” R D RES DEV KOBE STEEL LTD, vol. V 32, no. N 2, pp. 8–12, 1982.

[12] P. Reipert, “Optimization of an extremely light cast aluminium wheel rim.,” International Journal of Vehicle Design, 1985, doi: 10.1504/IJVD.1985.061385.

[13] J. A. Sherwood, B. K. Fussell, W. R. Edwards, T. S. Gross, and D. W. Watt, “Study of the pressure distribution on an aircraft tire–wheel interface,” J Aircr, vol. 32, no. 5, 1995, doi: 10.2514/3.46819.

[14] G. Machave, P. S. Sambhaji, and R. Kathar, “Study of Influrncr of Pressure and Load on Wheel Rim by Radial Fatigue Test,” Int J Eng Sci Res Technol, vol. 4, no. 2, pp. 298–303, 2015.

[15] U. Kocabicak and M. Firat, “Numerical analysis of wheel cornering fatigue tests,” Eng Fail Anal, 2001, doi: 10.1016/S1350-6307(00)00031-5.

[16] H. Shiobara, T. Akasaka, and S. Kagami, “Two-dimensional contact pressure distribution of a radial tire in motion,” Tire Sci Technol, 1996, doi: 10.2346/1.2137524.

[17] K. Ishihara and H. Kawashima, “Stress Evaluation of Automotive Steel Road Wheel under Radial Load,” Transactions of the Japan Society of Mechanical Engineers Series C, 1989, doi: 10.1299/kikaic.55.1254.

[18] S. Bošnjak, Z. Petković, N. Zrnić, M. Pantelić, and A. Obradović, “Failure analysis and redesign of the bucket wheel excavator two-wheel bogie,” Eng Fail Anal, 2010, doi: 10.1016/j.engfailanal.2009.09.007.

[19] N. Satyanarayana and C. Sambaiah, “Fatigue Analysis of Aluminum Alloy Wheel Under Radial Load,” International Journal of Mechanical and Industrial Engineering, 2012.

[20] W. Wang, S. Yan, and Y. Zhao, “Numerical and experimental studies of a radial truck tire with tread pattern,” Simulation, vol. 91, no. 11, pp. 970–979, 2015, doi: 10.1177/0037549715608434.

[21] N. Korunović, M. Trajanović, and M. Stojković, “FEA of tyres subjected to static loading,” Journal of Serbian Society for Computational Mechanics, 2007.

[22] J. A. Guinea García-Alegre, “Numerical study of aluminum wheels subjected to biaxial fatigue test,” Politecnico di Milano, 2017.

[23] X. Zhang, S. Rakheja, and R. Ganesan, “Stress analysis of the multi-layered system of a truck tire,” Tire Science and Technology. 2002. doi: 10.2346/1.2135257.

[24] L. Renčín, A. Polcar, and F. Bauer, “The effect of the tractor tires load on the ground loading pressure,” Acta Universitatis Agriculturae et Silviculturae Mendelianae Brunensis, 2017, doi: 10.11118/actaun201765051607.

[25] W. Wang, S. Yan, and S. Zhao, “Experimental verification and finite element modeling of radial truck tire under static loading,” Journal of Reinforced Plastics and Composites, 2013, doi: 10.1177/0731684412474998.

[26] J. J. Castillo Aguilar, J. A. Cabrera Carrillo, A. J. Guerra Fernández, and S. Postigo Pozo, “Optimization of an optical test bench for tire properties measurement and tread defects characterization,” Sensors (Switzerland), 2017, doi: 10.3390/s17040707.

[27] P. Sujin, Y. Wansuk, C. Jinrae, and K. Beomsoo, “Pressure-sensing pad test and computer simulation for the pressure distribution on the contact patch of a tyre,” Proceedings of the Institution of Mechanical Engineers, Part D: Journal of Automobile Engineering, 2007, doi: 10.1243/09544070JAUTO382.

[28] K. Cosseron, D. Mellé, J.-F. Diebold, F. Hild, and S. Roux, “Optimized gauging for tire-rim loading identification,” European Journal of Mechanics - A/Solids, 2020, doi: 10.1016/j.euromechsol.2020.104192.

[29] S. Medvedev, R. Ivanets, U. Ausianka, A. Kasperovich, V. Mozgalev, and N. Prokopchuk, “Coupled thermomechanical computational solutions for stationary and dynamics rocking of all-metal steel belted tyres,” in Procedia Engineering, 2016. doi: 10.1016/j.proeng.2016.01.166.

[30] Y. Deng, Y. Zhao, F. Lin, Z. Xiao, M. Zhu, and H. Li, “Simulation of steady-state rolling non-pneumatic mechanical elastic wheel using finite element method,” Simul Model Pract Theory, 2018, doi: 10.1016/j.simpat.2018.04.001.

[31] E. M. Adigio and E. O. Nangi, “Computer Aided Design and Simulation of Radial Fatigue Test of Automobile Rim Using ANSYS,” IOSR Journal of Mechanical and Civil Engineering, 2014, doi: 10.9790/1684-11146873.

[32] J. Schijve, Fatigue of structures and materials. 2009. doi: 10.1007/978-1-4020-6808-9.

[33] “Total Materia.” Accessed: Feb. 10, 2020. [Online]. Available: https://www.totalmateria.com

[34] “Material fatigue.” Accessed: Feb. 10, 2020. [Online]. Available: www.comsol.it/multiphysics/material-fatigue

[35] F. M. Santiciolli, R. Möller, I. Krause, and F. G. Dedini, “Simulation of the scenario of the biaxial wheel fatigue test,” Advances in Engineering Software, 2017, doi: 10.1016/j.advengsoft.2017.08.006.

[36] G. Wang, H. Sun, J. Li, and R. Chai, “Study on biaxial fatigue life test and FEA analysis of the steel wheel,” in ICIC 2010 - 3rd International Conference on Information and Computing, 2010. doi: 10.1109/ICIC.2010.330.

[37] C. C. Osgood, “Prediction of fatigue life,” in Fatigue Design, Elsevier, 1982, pp. 41–404. doi: 10.1016/b978-0-08-026167-6.50009-6.

[38] “Calculating damage with Miner’s Rule.” Accessed: Feb. 10, 2020. [Online]. Available: https://community.sw.siemens.com/s/article/calculating-damage-with-miner-s-rule

[39] B. L. Barcelos and E. S. Palma, “Fatigue analysis of a bucket wheel by using Linear Elastic Fracture Mechanics,” Eng Fail Anal, 2020, doi: 10.1016/j.engfailanal.2020.104824.

[40] “Random Load Fatigue.” Accessed: Feb. 10, 2020. [Online]. Available: https://www.comsol.it/blogs/random-load-fatigue/

[41] “The Strain Life Approach.” [Online]. Available: https://community.sw.siemens.com/s/article/The-Strain-Life-Approach

[42] “History of Fatigue.” Accessed: Feb. 10, 2020. [Online]. Available: https://community.sw.siemens.com/s/article/history-of-fatigue

[43] J. Stearns, T. S. Srivatsan, X. Gao, A. Prahash, and P. C. Lam, “Analysis of Stress and Strain Distribution in a Vehicle Wheel: Finite Element Analysis Versus the Experimental Method,” J Strain Anal Eng Des, 2005, doi: 10.1243/030932405X30786.

[44] Y. Morita, H. Kawashima, and K. Ishihara, “Induced stress evaluation of automotive steel road wheel during endurance tests,” Sumitomo Metals, 1989.

Paper submitted: 11.12.2023.

Paper accepted: 11.03.2024.